

Article

Multi-Time Scale Optimal Scheduling Model of Wind and Hydrogen Integrated Energy System Based on Carbon Trading

Xuan Wen ^{1,2,*}, Bo Sun ¹, Bing Gu ^{1,2} and Yan Lv ¹

¹ State Key Laboratory of Power Grid Safety and Energy Conservation (China Electric Power Research Institute), Beijing 100192, China

² School of Information Engineering, Nanchang University, Nanchang 330038, China

* Correspondence: ncuwenx@163.com

Abstract: In the context of carbon trading, energy conservation and emissions reduction are the development directions of integrated energy systems. In order to meet the development requirements of energy conservation and emissions reduction in the power grid, considering the different responses of the system in different time periods, a wind-hydrogen integrated multi-time scale energy scheduling model was established to optimize the energy-consumption scheduling problem of the system. As the scheduling model is a multiobjective nonlinear problem, the artificial fish swarm algorithm–shuffled frog leaping algorithm (AFS-SFLA) was used to solve the scheduling model to achieve system optimization. In the experimental test process, the Griewank benchmark function and the Rosenbrock function were selected to test the performance of the proposed AFS-SFL algorithm. In the Griewank environment, compared to the SFLA algorithm, the AFS-SFL algorithm was able to find a feasible solution at an early stage, and tended to converge after 110 iterations. The optimal solution was -4.83 . In the test of total electric power deviation results at different time scales, the maximum deviation of early dispatching was 14.58 MW, and the minimum deviation was 0.56 MW. The overall deviation of real-time scheduling was the minimum, and the minimum deviation was 0 and the maximum deviation was 1.89 WM. The integrated energy system adopted real-time scale dispatching, with good system stability and low-energy consumption. Power system dispatching optimization belongs to the objective optimization problem. The artificial fish swarm algorithm and frog algorithm were innovatively combined to solve the dispatching model, which improved the accuracy of power grid dispatching. The research content provides an effective reference for the efficient use of clean and renewable energy.

Keywords: carbon trading; integrated energy system; time scale; dispatch



Citation: Wen, X.; Sun, B.; Gu, B.; Lv, Y. Multi-Time Scale Optimal Scheduling Model of Wind and Hydrogen Integrated Energy System Based on Carbon Trading. *Processes* **2023**, *11*, 344. <https://doi.org/10.3390/pr11020344>

Academic Editors: Dapeng Zhang, Qiangda Yang and Yuwen You

Received: 23 December 2022

Revised: 14 January 2023

Accepted: 18 January 2023

Published: 20 January 2023



Copyright: © 2023 by the authors. Licensee MDPI, Basel, Switzerland. This article is an open access article distributed under the terms and conditions of the Creative Commons Attribution (CC BY) license (<https://creativecommons.org/licenses/by/4.0/>).

1. Introduction

The world's energy is gradually declining and environmental problems are growing. Effective exploration of new energy is an important strategy to solve development problems. The carbon trading mechanism is an effective strategy to give consideration to economic and environmental development, to analyze regional carbon emissions on the basis of the carbon trading theory, and to seek ways to reduce carbon emissions on the premise of safeguarding regional economy. The wind-hydrogen integrated energy system is a user oriented new microenergy system. On the basis of meeting low-carbon transactions, the integrated energy system (IES) has been applied in some parts of China as a demonstration. Wind-hydrogen integrated energy systems are a kind of IES system, and their energy is mainly wind energy and hydrogen energy. The key point lies in the mutual supplementation of multiple energy sources. Through the complementary role of multiple energy sources, the potential and the advantages of various energy sources can be fully exerted, thus improving the stability and security of the power system. The goal of integrated energy systems is to realize the conversion and storage of multiple energy sources and meet

the flexible dispatching requirements of renewable energy power systems. Under the theory of carbon trading, the optimization of integrated energy-system scheduling can effectively balance the relationship between system energy consumption, economy, and system stability. Simultaneously, integrated energy-system scheduling optimization is beneficial to minimizing system energy consumption and carbon emissions, which is critical to fostering sustainable economic growth. The scheduling mechanism of wind-hydrogen integrated energy systems directly affects the stability and energy-consumption effect of the system. Comprehensive analysis of the relevant factors affect the energy system and establishment of a multi-time scale optimal scheduling model. Considering the multiobjective optimization problem, neural network technology was innovatively used to solve the model so as to achieve the energy conservation and emissions reduction goal of power grid dispatching.

2. Literature Review

In recent years, global environmental issues have attracted the attention of the public. In the context of carbon energy saving, new green energy such as wind energy and hydrogen energy has received a lot of interest with both national and international experts have presenting effective analyses on the topic. Rezaei et al. studied the prospects of wind energy and hydrogen energy, including the cost of wind power generation, the cost of hydrogen fuel, rates of return, and other parameters. Considering the inclusion of many uncertainties in the study, both the performance-related degradation rates of wind turbines and the monetary value-related degradation rates were investigated. From this research, it was found that the hydrogen production system's use time was generally between 3.91–8.41 years, and each target's matching rate of return was calculated [1]. Solomin et al. conducted research on the power grid project in the Arctic region. The construction goals of the project mainly considered wind energy and hydrogen energy. The hydrogen module was used as an uninterruptible power supply and can be obtained in all regions of the world. The environmental protection characteristics and reliability of hydrogen energy enable it to meet the environmental protection objectives as well as the power demand of the region. The project realized the management and monitoring of power generation and hydrogen storage through a remote terminal system. The final results of the project showed that the project could provide reliable, stable, and environmentally friendly functional requirements while also maintaining its affordability for consumers in the region [2]. Akhavan Shams and Ahmadi emphasized that the world is in an energy crisis, and renewable energy will be the key to solve the problem. Therefore, they proposed a grid-connected photovoltaic system for educational buildings, and the relationship model of renewable energy generation cost was established. They considered the environmental penalties and examined the link between important influencing elements and prices. Their experimental results showed that renewable energy did not meet the economic requirements, and if households use storage systems to store electricity, battery packs have advantages over combustion batteries [3]. Ozturk and Dincer found that intermittent fluctuations are common in renewable energy. A hydrogen battery is a kind of renewable energy with potential for development. In order to improve the renewability of fuel, Ozturk and Dincer compared several hydrogen production methods from the aspect of cost efficiency and the environment. The results showed that the use of polymer electrolyte membrane electrolyzers for hydrogen production has more obvious advantages, and at the same time, the overall cost of hydrogen production based on geothermal energy was the lowest [4]. Ishaq et al. found that developing new energy will be the key to solving the problem. Research on traditional hydrogen production and the hydrogen production from wind energy and solar energy is intermittent. Therefore, Ishaq et al. constructed an evaluation model based on cost, infrastructure, and efficiency, etc., to compare various hydrogen production systems. Finally, Ishaq et al. summarize the opportunities and challenges faced by hydrogen production [5]. Ishaq and Dincer proposed a hybrid photovoltaic structure for system function analysis, which is used to solve the high-energy consumption of hydrogen production and optimize the hydrogen

production process. Considering that the power of a wind farm is affected by wind speed, solar energy depends on the intensity of solar radiation, then the designed system mainly met the relevant requirements of hydrogen production and adopted the cascade hydrazine synthesis system to achieve a high conversion. The final experiment showed that the proposed method was feasible [6].

Reasonable scheduling optimization of the energy system can achieve the balance of power-grid-energy consumption and performance. Lin et al. studied the virtual power plant technology that can better integrate power resources. They analyzed the dispatching relationship between the distributed generation units and the power grid system to optimize system energy consumption, and they proposed a virtual power plant economic dispatching scheme. Neural network technology was used to train and optimize the correlation number to achieve a more economical scheduling scheme. Finally, experimental verification showed that the scheme has good performance [7]. Xu et al. proposed a power dispatching scheme based on time distribution, taking the energy hub center as the system's decision-making center. Through this scheme, the power supply, transmission and coupling relationship were effectively optimized to better realize the synergy of multienergy networks. However, the distributed time scheduling strategy faced optimization problems, so the problem was transformed into mixed integer second-order cone programming, and the problem was handled by sequential second-order cone programming. Finally, the scheme was confirmed to have an excellent performance effect and reduce system energy consumption [8]. Pan et al. found that the renewable integrated energy system had a good development trend and they constructed a comprehensive energy planning model based on hydrogen production and hydrogen storage technologies. A robust strategy was adopted to optimize the system load problem, and the feasibility of the scheme was verified by experiments [9]. Dou et al. studied the existing integrated energy system and found that the traditional fixed-time scheduling scheme was not suitable for the relevant characteristics of the transient network and would lead to uneconomic problems in the energy system. So, a scheduling scheme based on model predictive control was proposed. First of all, the model of the integrated energy subsystem of electric power, gas, and heat and the multienergy load was built, and then an optimization method was proposed to optimize the scheduling model through the trajectory deviation control and energy control in MPC. Finally, the experiment proved that the proposed optimal scheduling scheme could be applied to various scenarios and could effectively save system energy consumption and reduce costs [10,11].

It is evident that the world is facing environmental problems and petrochemical depletion and the development of renewable energy will be the key to solving the energy crisis. However, the integrated energy system is faced with problems such as scheduling and unstable performance output. Compared with the scheme proposed by Rezaei et al. and Solomin et al., using a more intelligent multiobjective AFS-SFLA algorithm model for an optimal solution could better achieve the balance of system energy consumption and performance [1,2], and achieve the goal of system energy conservation and emissions reduction.

3. Construction of a Multi-time Scale Optimal Dispatch Model for a Wind-Hydrogen Integrated Energy System

3.1. Construction of Energy System Equipment Model

The optimization of integrated energy-system dispatching is one of the important tasks for power grids to achieve energy conservation and emissions reduction. Due to the instability of energy transmission during the acquisition of wind and hydrogen energy, this specific randomness and uncertainty has led to instability and excessive energy consumption in the energy scheduling process of an integrated energy system. Therefore, the construction of wind and hydrogen systems needs to meet the requirements of carbon emissions and environmental protection. The storage of electric energy and heat energy should

be fully considered in the system construction, as shown in Figure 1, which illustrates the schematic diagram of the system structure.

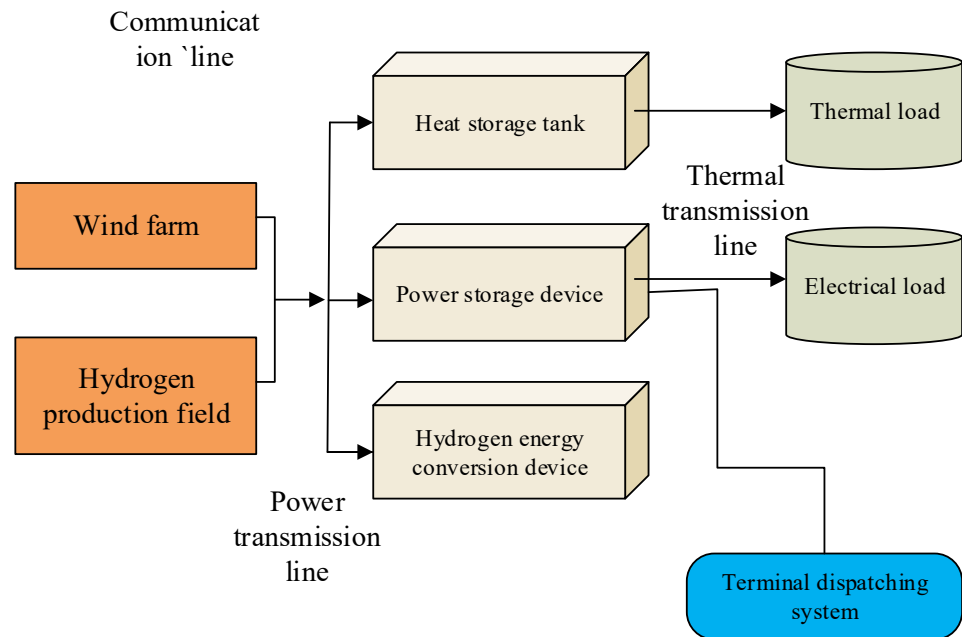


Figure 1. Structural diagram of wind-hydrogen integrated energy system.

Under the low-carbon emission policy, the Chinese government actively advocates for the development of energy-saving and environmentally friendly new energy sources, among which wind energy and hydrogen energy are rich in resources and have high-development potential [12]. A variety of distribution strategies are used to describe the random distribution relationship of wind speed and since there is no unified hydrogen production plan, the relevant factors are quantified. [13]. This research proposes a carbon emission method of progressive mixed allocation based on the above-mentioned distribution decision making. Progressive mixed allocation refers to the allocation method that combines free and paid allocation schemes with its distinctive characteristic that the scheme can increase its allocation ratio over time. The typical distribution curve of wind speed probability is shown in Equation (1).

$$F_{weibull}(v) = 1 - \exp[-(\frac{v}{c})^k] \tag{1}$$

In Equation (1), c represents the distribution parameter, v represents the wind speed, k represents the shape parameter of the wind, $k \in [1.8, 2.3]$. In the Weibull distribution description, the wind trajectory is expressed as shown in Equation (2).

$$k = (\frac{\sigma}{\mu})^{-1.086} \tag{2}$$

In Equation (2), σ represents the approximate operator, μ represents the average speed of the wind, and the output relationship of wind power is expressed as shown in Equation (3).

$$p_{wt}(v) = \begin{cases} 0 & 0 \leq v \leq C_{ci} \\ (A + Bv + Cv^2) & V_{ci} \leq v \leq V_r \\ p_r & V_r \leq v \leq V_{co} \\ 0 & v \geq V_{co} \end{cases} \tag{3}$$

In Equation (3), V_{co} represents the cut-out wind speed, V_{ci} represents the cut-in wind speed, p_r represents the rated power of the unit, and V_r represents the rated wind speed.

A , B , and C represent the characteristic parameters of the wind curve, and the value will have a direct impact on the performance of the wind turbine [14]. In order to better describe the economic benefits of wind power generation, factors such as cost, income, and environmental protection benefits were comprehensively considered, and the operating life of the wind turbine was calculated.

$$C_{wt} = \frac{N_{wt}C_{wB} + \sum_{Y=1}^{20} [(1 - \beta_{CPI})^{Y-1} C_{WME}]}{20 \times N_{wt} T_{wmax} p_{wN}} - B_{subsidy} \quad (4)$$

In Equation (4), C_{wB} represents the unit cost of the fan, N_{wt} represents the total number of fans, β_{CPI} represents the price increase coefficient, T_{wmax} represents the annual load time of the fan, C_{WME} represents the annual use cost of the fan, $B_{subsidy}$ represents the state subsidy, and Y represents the life of the fan. In addition, the cost of wind curtailment should also be considered, as shown in Equation (5).

$$C_{wd}(t) = \sum_{i=1}^{N_{wt}} [p_{wt}(t) - p_{wtu}(t)] \times C_{wt} \times t \quad (5)$$

In Equation (5), $p_{wt}(t)$ represents the total power of the wind turbine at the moment t , N_{wt} represents the total number of fans, and $p_{wtu}(t)$ represents the power used at the moment t .

Although the use of renewable energy has reduced the use of carbon-emitting units in the wind-hydrogen comprehensive energy system investigated in this study, thermal power still occupied a major source of output. The energy output of thermal power plants mainly relies on the combustion of nonrenewable energy sources to generate heat for power generation. The unit power generation model of a thermal power plant is shown below.

$$P_{fh}(t) = \delta C_{co}(t) \quad (6)$$

In Equation (6), $P_{fh}(t)$ represents the total output power of the thermal power generating set at a moment t , δ represents the energy conversion rate of the motor, and $C_{co}(t)$ represents the fuel consumption at a given moment t .

In addition to the thermal power generation unit, the carbon emission unit model in the wind-hydrogen comprehensive energy system studied here also included a gas turbine device that converted natural gas into electrical energy. The power model of the gas turbine is shown below.

$$P_{gt}(t) = f_g S_g E \left(1 - 1/\gamma_i^{r_i} \right) \sigma_i \quad (7)$$

In Equation (7), $P_{gt}(t)$ represents the total output power of the gas turbine at that moment t , f_g represents the flow rate of the gas, S_g represents the average value of the specific heat capacity of the fuel at constant pressure, E represents the gas temperature at the outlet of the gas turbine, γ_i represents the turbine expansion ratio, and r_i represents the average specific heat ratio of the gas.

In a wind and hydrogen integrated energy system, the storage system needs to maintain the uninterrupted power supply demand of the integrated system and its stability is key. Generally, the storage system adopts a lead storage battery, which is safer, more stable, and less expensive, as the preferred equipment for the basic unit of the distributed power supply [15]. The energy storage relationship is expressed in Equation (8).

$$E_{ees}(t) = 1 - a_{es} E_{ees}(t - 1) + (p_{es,c}(t) \beta_{es,c} - p_{es,f}(t) / \beta_{es,f}) \Delta t \quad (8)$$

In Equation (8), a_{es} represents the self-discharge rate, E_{ees} represents the battery energy storage, $p_{es,c}$ represents the charging power of the charging group, $p_{es,f}$ is the charging power of the discharging group, $\beta_{es,c}$ represents the charging efficiency, and $\beta_{es,f}$ represents

the discharging efficiency. In a storage system, the energy and power of the system change with time. By dynamically absorbing and releasing energy, the storage system can reduce the dispatch risk caused by the incorrect prediction of wind and hydrogen energy and ensure system stability [15].

The heat storage tank is a key part of the system and it ensures the balance of the heat energy of the system by processing the heat source. The schematic is shown in Figure 2.

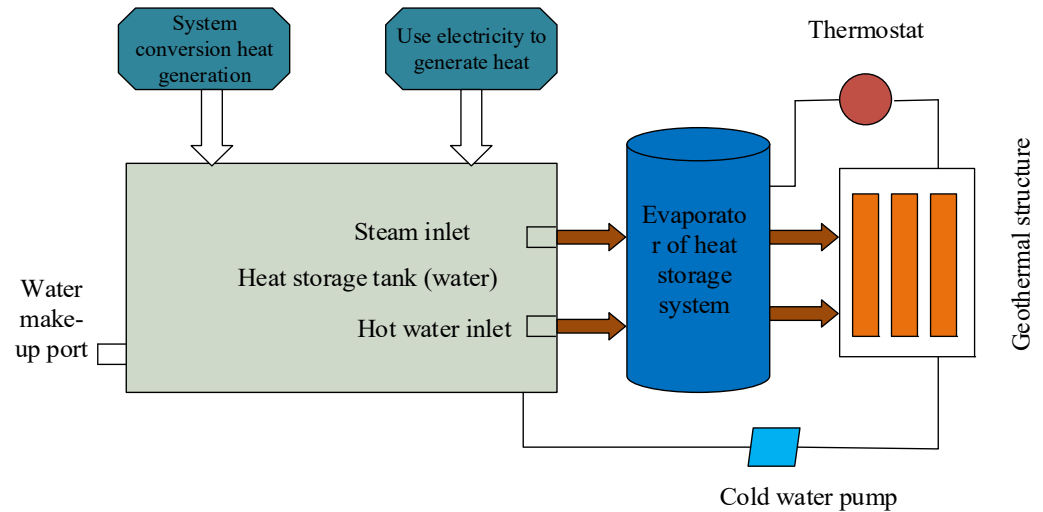


Figure 2. Structural diagram of a heat storage tank.

The absorbing capacity of the heat storage tank is related to its placement. When the integrated energy system is under a high load, a large amount of heat will be generated. At this moment, the heat storage tank needs to be used to balance the heat energy. The heat storage expression of the heat storage tank is as shown in Equation (9).

$$Q_{hs}(t) = (1 - \gamma_{hs})Q_{hs}(t - 1) + [H_{hs,in}(t)\mu_{hs,in}(t) - H_{hs,out}(t)/\mu_{hs,out}] \Delta t \quad (9)$$

In Equation (9), γ_{hs} represents the heat dissipation loss rate, Q_{hs} represents the heat storage capacity, $H_{hs,in}$ represents the heat absorption power, $H_{hs,out}$ represents the heat release power, $H_{hs,out}$ represents the heat absorption efficiency, and $\mu_{hs,out}$ represents the heat release efficiency.

3.2. Hybrid Algorithm Model Construction

The scheduling of a wind-hydrogen integrated energy system is a multiobjective, nonlinear problem, and effective system scheduling is the key to solve the problem. The general optimization algorithm could not solve the multiobjective calculation problem, so the hybrid artificial fish school shuffled frog leading algorithm (AFS-SFLA) was used to solve the high-latitude problem of the system [16]. The fish swarm algorithm is a kind of swarm intelligence optimization method, which simulates the foraging behavior of fish. The principle of the fish swarm algorithm is shown in Figure 3.

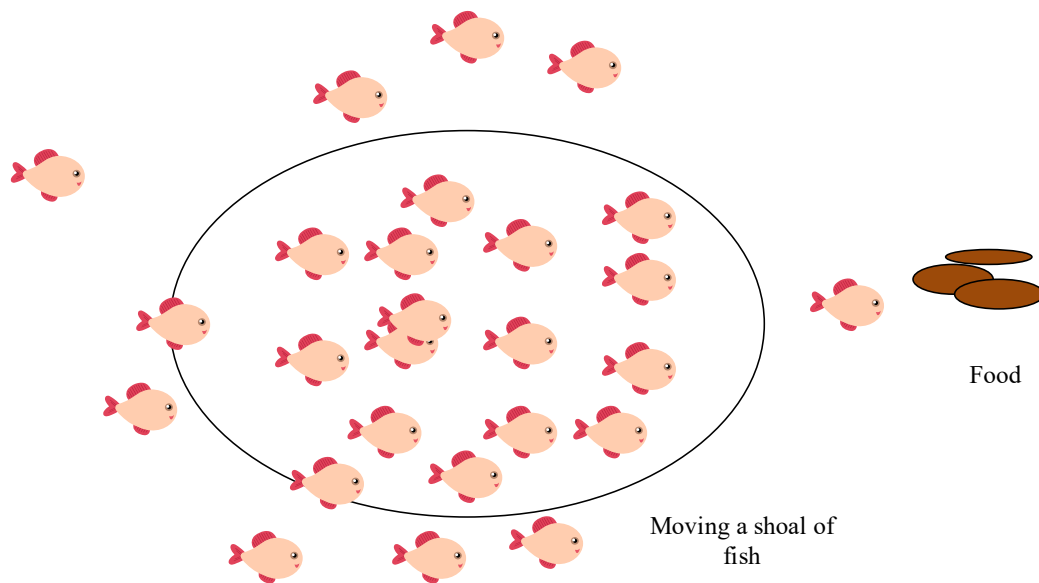


Figure 3. The principle of the fish swarm algorithm.

The state of the artificial fish is defined as X_i , in the foraging behavior, any arbitrary state is defined within the range that it can forage X_j , the goal of the fish school is to seek the maximum value ($Y_i < Y_j$), and the fish school moves in the X_j direction, or selects a X_j state arbitrarily. It repeats m times, and if the requirements are not met, it moves forward arbitrarily. In the clustering behavior, the current range is studied. The number of peers in the research range is n_f , and the central location is Y_j . If it exists $Y_c/n_f > \delta Y_i$, it δ indicates the degree of crowding, which means that the central area is not crowded and there is more food. The rear-end behavior mainly refers to testing the number of partners in the current range and the n_f largest partner in X_j the center of the area Y_j . If there is $Y_i/n_f > \delta Y_i$, it means that there is more food in the companion position, and it is not crowded. In the random behavior of artificial fish swarms, the fish shoals are randomly selected within the range, and they can move forward in this direction. The expression is shown in Equation (10).

$$X_{i\text{Inex}} = X_i + r + Vi \quad (10)$$

In Equation (10), Vi represents the perceivable distance of the artificial fish, and the r value is $[-1, 1]$. In the artificial fish swarm, any fish is a solution, and the best foraging area can be found by means of fish swarm communication, and then the global optimal solution can be found.

The leapfrog algorithm is a new swarm intelligence algorithm, which is a particle swarm optimization method that combines genetic behavior and animal behavior. The classification and exchange of information were realized through the behavior of frog populations, and a global optimal solution was sought [17,18]. It defined the number of SFLA population groups as m , and the number of frogs in each group as n . In the initialized frog population, the number of frogs generated is F , denoted as $P = (P_1, P_2, \dots, P_F)$, where P_i is the number of solutions, the value is $(0 \leq i \leq F)$, and $p_i = (p_{i1}, p_{i2}, \dots, p_{id})$, d represents the number of solutions, and each frog represents a solution. In the global optimization, the fitness value is $fitness(p_i)$, the calculated first fitness value corresponds to the P_i global optimal frog, and the frogs were sorted into p the middle, p the first frog was placed into one group, and the frogs were sorted in turn m into groups. A local search was performed on each subgroup that had been divided, and the set maximum number of iterations was satisfied, then the search was ended. Because of the local optimal problem in the survey of artificial fish stocks, the AFS-SFLA algorithm was proposed by combining the above two algorithms. The specific flow of the algorithm is shown in Figure 4.

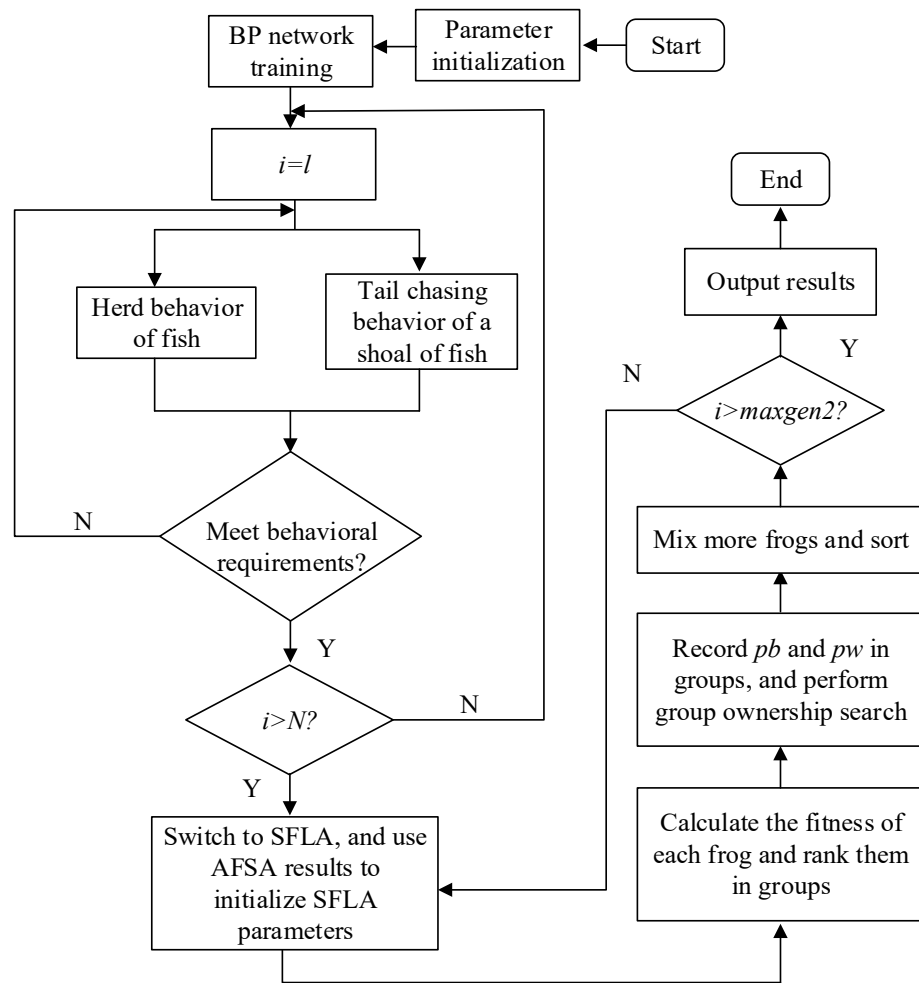


Figure 4. Schematic diagram of AFS-SFLA algorithm.

The main idea of the AFS-SFLA algorithm was to use the artificial fish swarm to obtain the fish swarm as the initialization parameter of the frog leaping algorithm, and k assign the times of the total number of frogs to the frog population, among which $0 < k < 1$. Then the fitness of each frog was calculated, the optimal solution frog was recorded, the position of the worst frog was grouped and adjusted, if it exists $ii > \maxgen2$, and training was completed. The ii loop variable $\maxgen2$ represents the maximum iteration.

3.3. Scale Scheduling Model for a Wind-Hydrogen Integrated System

System consumption is a key indicator of a system. Considering the interference of the renewable energy load and various factors of system scheduling, the AFS-SFLA algorithm was used to determine the optimal scheduling scheme of the system and build a multi-time scheduling model of the system [19]. Among them, in the objective calculation of the objective function, the carbon-transaction-cost based on the ladder-type carbon trading price mechanism is defined as $C_{tp}(t)$, the equipment maintenance fee is defined as $C_{om}(t)$, the environmental pollution fee $C_{et}(t)$ is $C_{wc}(t)$ as $C_{fu}(t)$. Adding wind energy and hydrogen energy disposal costs into the objective function will allow a more intuitive analysis of the electricity consumption capacity of the integrated energy system.

$$\min F = \sum_{t=1}^T (C_{fu}(t) + C_{et}(t) + C_{wc}(t)) \Delta t \quad (11)$$

In Equation (11), T represents the total time period of the system scheduling, where F represents the operating cost of the system for one day, Δt is the scheduling change time, and the equipment maintenance cost is expressed in Equation (12).

$$C_{om}(t) = \sum_{i=1}^{N_{om}} K_{om,i} |p_i(t)| \quad (12)$$

In Equation (12), $K_{om,i}$ represents the maintenance cost of the equipment unit, N_{om} represents the number of equipment units, and $p_i(t)$ the output power of the equipment category i at the moment t . The expression of environmental pollution cost is shown in Equation (13).

$$C_{et} = \sum_{j=1}^m V_j p_{i,t} \quad (13)$$

In Equation (13), $j = 1$ represents carbon dioxide, $j = 2$ represents sulfide, $j = 3$ represents nitrogen oxide, $p_{i,t}$ represents the amount of pollutant discharge of equipment items i , V_j represents the penalty of the first pollutant, and j represents the type of pollutant. In an integrated energy system, constraints such as power coefficients and equipment operation need to be fully considered.

In the IES system investigated in this study, each carbon emission system contained the limit constraints of each production machine. The output limit constraint expression of each unit can be seen in Equation (14).

$$\left\{ \begin{array}{l} P_{firek,\min} \leq P_{firek}(t) \leq P_{firek,\max} \\ P_{hk,\min} \leq P_{fire}(t) - P_{fire}(t-1) \leq P_{hk,\max} \\ P_{wind,\min} \leq P_{wind}(t) \leq P_{wind,\max} \\ P_{nig,\min} \leq P_{nig}(t) \leq P_{nig,\max} \\ P_{gtk,\min} \leq P_{gtk}(t) \leq P_{gtk,\max} \end{array} \right. \quad (14)$$

In Equation (14), $P_{firek,\min}$, $P_{firek,\max}$ represent the minimum and maximum value of the thermal power unit at the time of k , respectively. $P_{hk,\min}$, $P_{hk,\max}$ represent the minimum and maximum ramp rate of the thermal power group at the time of k , respectively. $P_{wind,\min}$, $P_{wind,\max}$ represent the minimum and maximum output of the wind turbine, respectively. $P_{nig,\min}$, $P_{nig,\max}$ represent the minimum and maximum value of the photovoltaic output, respectively. $P_{gtk,\min}$, $P_{gtk,\max}$ represent the minimum and maximum value of the gas turbine output at the time of k , respectively. At the same time, in the energy storage system, it was usually necessary to ensure the life and working efficiency of the battery, and the battery charging limit and discharge depth are shown in Equation (15).

$$E_c SOC_{\min} \leq E_{ees}(t) \leq E_c SOC_{\max} \quad (15)$$

In Equation (15), $E_c SOC_{\max}$ represents the maximum state of charge of the battery, $E_c SOC_{\min}$ represents the minimum state of charge of the battery, and E_c represents the rated capacity of the battery. In the operation of the heat storage tank, it was also necessary to fully consider the heat storage range in each period, and the operational constraints of the heat storage tank are shown in Equation (16).

$$Q_{\min} < Q_{hs}(t) \leq Q_{\max} \quad (16)$$

In Equation (16), Q_{\max} represents the maximum thermal storage energy of the thermal storage tank, Q_{\min} represents the minimum thermal storage energy of the thermal storage tank, and $Q_{hs}(t)$ represents the heat stored in the thermal storage tank at the moment t . In the integrated energy system, it was also necessary to consider the electrical power balance

constraints, including the load balance of the wind turbines, hydrogen generating units, and electrical energy storage equipment.

$$p_{load}(t) = p_{hs}(t) + p_{EES}(t) - p_{WT,use} - p_H(t) \quad (17)$$

In Equation (17), $p_{EES}(t)$ means that the battery is producing electricity at the moment t , $p_{hs}(t)$ is the system use of the electricity load at the moment t , $p_{WT,use}$ is the wind power that the system is consuming, and $p_H(T)$ represents the hydrogen electricity that the system is consuming.

A real-time scheduling plan was established on the basis of the above. The first step was to add a real-time carbon emission feedback link to the intraday scheduling plan. The real-time environmental assessment model of carbon emission in IES is shown in Equation (18).

$$\begin{cases} Q_{min}(t) \leq Q_{HP}(t) + Q_{RP}(t) \leq Q_{target}(t) \\ Q_{realtime}(t) = Q_{HP}(t) + Q_{RP}(t) + Q_{WG}(t) \\ Q_{realtime}(t) \leq Q_p(t) \end{cases} \quad (18)$$

In Equation (18), $Q_{min}(t)$ represents the emission amount of the carbon emission unit at a moment under the condition of stable operation of the system, $Q_{target}(t)$ represents the real-time carbon emission target of the carbon emission unit at a given moment t , $Q_{realtime}(t)$ represents the real-time carbon emission of the IES system of the system at a given moment t , and $Q_p(t)$ represents the IES system in engraved carbon emission targets at the moment t .

The purpose of the system optimization scheduling model is to optimize parameters such as system electrical output, system electrical power consumption, and system heat dissipation power within 1 to 24 h. The real-time scheduling is mainly based on the daily scheduling, dynamic data adjustment and monitoring according to the forecast data set as expected, that $t = t_1$ is to say, the correction is the $t = t_1 + 1$ effect [20,21]. The final scheduling target is shown in Equation (19).

$$\begin{cases} -\Delta p^{\max} \leq (p^{real}(t) - p^{roll}(t)) \leq \Delta p^{\max} \\ \Delta p^{\max} \leq \varepsilon p^{\max} \end{cases} \quad (19)$$

In Equation (19), p^{real} represents the real-time dispatching output of the system equipment, p^{\max} represents the maximum value of the system output, and ε represents the constraint multiplier. Then the system multi-time scale optimization is shown in Figure 5.

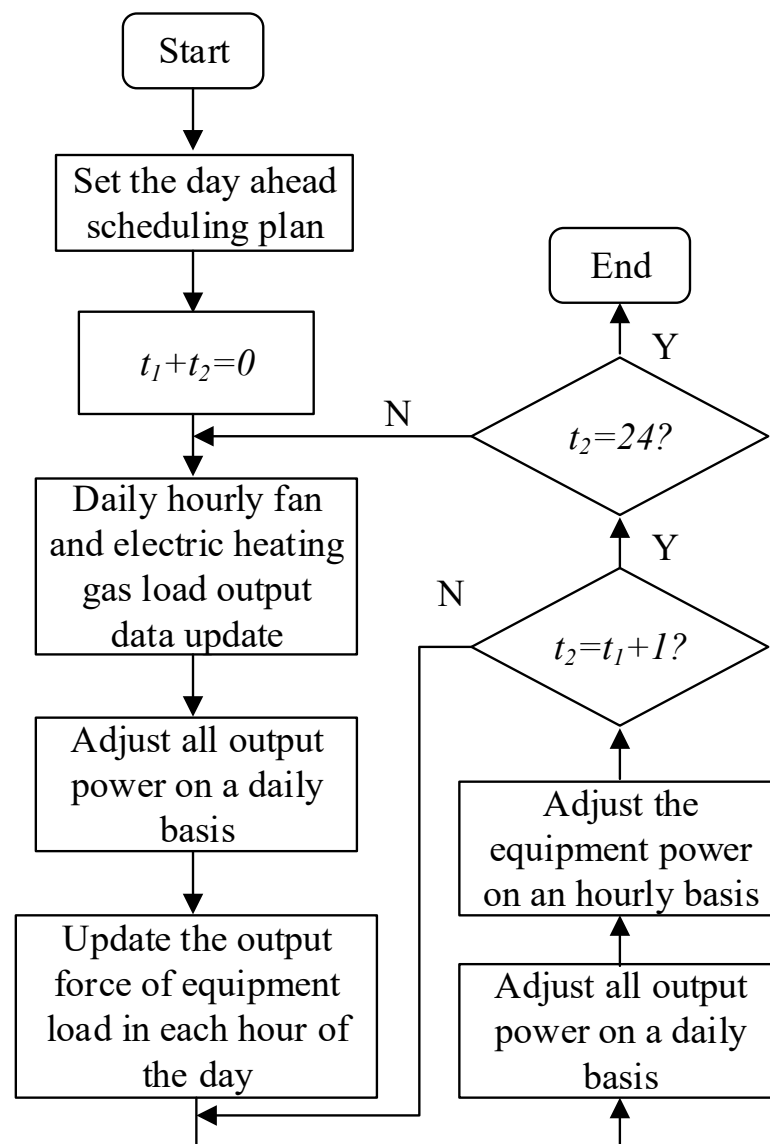


Figure 5. Multi-time scale optimization of energy system.

4. Performance Test of Optimal Dispatch Model for Wind and Hydrogen Integrated Energy Systems

In the experiment, a green renewable integrated energy system was selected as the experimental object, and the recorded parameters were selected as the experimental data. MATLAB and Yalmip were used to complete the experimental simulation test. In the algorithm performance test, the number of fish groups was set to 180, the number of population groups to 10, the step size to 0.1, and the constraint multiplier was set to 0.3 [22–24]. Considering the random interference of the integrated system, the algorithm interference was suppressed by different dimensions d . The Rosenbrock and Griewank benchmark functions were used to test the convergence performance of the algorithm. Figure A1 shows the test results under the two benchmark functions.

Figure A1a is the test result under the Griewank function. From the data in the figure, it can be seen that the SFLA algorithm has a clear trend of change in the first 100 iterations of the test. After 100 times, it tends to converge and falls into a local optimal solution, and the output value at this moment is -3.82 . The AFS-SFL algorithm is different from the SFLA algorithm. It can find a feasible solution in the early stages, and it tends to converge after 110 iterations. At that moment, the optimal solution is -4.83 . Figure A1b shows the test results under the Rosenbrock function. The SFLA algorithm did not perform well in the

early stage of iterative effects, there were obvious iterative changes at 180 iterations, and the optimal solution was obtained at 190 iterations. Compared with the SFLA algorithm, the AFS-SFLA algorithm performed better in the early iteration and tended to converge after 120 iterations. The output value of the function that found the optimal solution was -0.436 . It can be seen that the AFS-SFLA algorithm had a better iterative performance and optimization ability than the SFLA algorithm. At the same time, the algorithm performance was tested in dimension d . The results are shown in Table A1.

It can be seen from the data in Table A1 that the results of the two algorithms under the two benchmark functions were basically consistent, and the test accuracy is better when the dimension d is 50. At the same time, the AFS-SFLA algorithm used is better than the AFS algorithm. Therefore, d was taken as 50 and a further test was conducted [25]. Therefore, the AFS-SFLA algorithm was used to predict the typical daily electricity load power, thermal load power, and air intake power, as shown in Figure A2.

Figure A2 shows the typical daily load power prediction results. Figure A2a is the forecast result of the daily electricity load. The peak forecast of the daily electricity load was mainly at 8–12 h, reaching the peak at 17–20 h at night, and the electricity load power was 147 MW at 17 h. Figure A2b refers to the daily thermal load power results, from the data in the figure, the thermal power was mainly concentrated in 8–7, the power was 149–140 MW at that moment, and the thermal load power had a maximum value of 23, which was 151 MW. Figure A2c shows the power prediction results. From the prediction curve, it can be seen that the wind power was maintained in a high-energy consumption range between 0–8:00 in the morning and 22–24:00 in the evening, and the maximum value at 24:00 was 41 MW. During the daytime, the overall wind power was small and maintained in the range of 1–20 MW. During the integrated energy system operation of the system, it was necessary to consider the electric energy and thermal energy consumption caused by the operation of various equipment, including heat storage consumption, energy storage consumption, and operation consumption of wind and hydrogen equipment. The error results under different time periods are shown in Table A2.

Table A2 shows the forecast errors for different time periods. From the data in Table A2 it can be seen that in the short-term forecast, the forecasts of thermal load, electrical load, and wind power output power consumption were all high, with 5%, 4%, and 19%, respectively. In the short-term expansion, the forecasts for thermal load, electrical load, and wind power output and power consumption were 1%, 2%, and 8%, respectively, and the three forecast indicators for ultra-short-term forecasts were 0.4%, 0.3%, and 2.1%, respectively. It can be seen that although the AFS-SFLA algorithm has excellent prediction performance, the overall prediction accuracy decreases with the extension of the prediction time. Therefore, adopting a real-time scheduling strategy to dynamically adjust the system scheduling in a short time is more in line with the requirements of the integrated energy system [26–28]. Figure A3 shows the output results of combined heat and power and wind power consumption in each period.

Figure A3a shows the output power results of the CHP. The overall difference between day-to-day scheduling, rolling scheduling, and real-time scheduling was not large. Especially in the time interval between 18 and 24, the three different types of scheduling data were basically consistent. However, in general, the output power of day-ahead scheduling was higher than that of rolling scheduling and real-time scheduling, with the error between rolling scheduling and real-time scheduling being about 0.05%, indicating that both rolling scheduling and real-time scheduling had better scheduling performance. Figure A3b shows the output power results of the fans. The power variation curves of the fans at different time periods under the rolling scheduling and real-time scheduling were basically the same, the error was about 0.06%, and the overall curve fluctuation was small. However, the day-to-day scheduling fluctuated greatly between the time period 0–3 and the time period 20–22, and the overall output of power consumption of the day-to-day scheduling scheme was relatively high. At 12:00, the output power of day-ahead dispatch, rolling dispatch, and real-time dispatch were 14.6 MW, 2.3 MW, and 2.2 MW, respectively. It can be seen

that the time-scale scheduling scheme had lower power consumption and stronger system stability than the traditional day-ahead scheduling scheme. Table A3 shows the electrical consumption test results of the multiperiod integrated energy system.

From the data in Table A3, it can be concluded that the wind power consumption of different time-scale dispatching schemes was different. The daily power dispatch, rolling dispatch, and real-time dispatch of wind power consumption were 341.45 MW·h, 342.54 MWh, and 350.64 MW·h, respectively. The power consumption performance of the dispatching scheme was improved by 3.145% compared with the previous dispatching scheme. Among them, the electricity consumption of multiple time scales was 350.64 MW, which was 9.19/MW·h more than the previous dispatch, indicating that the multi-time scale scheme had better wind power consumption performance. Figure A4 shows the deviation results of the total electrical power and total thermal power deviation of the system at each time scale.

Figure A4a shows the results of the total electric power deviation for each time period. It can be seen from the graph data that the overall deviation of day-ahead scheduling was relatively large compared with the rolling scheduling and real-time scheduling. The simulation test of AFS-SFLA algorithm shows that the maximum deviation of day-ahead scheduling was 9.85 MW, the maximum deviation of rolling scheduling was 5.95 MW, and the real-time scheduling deviation was the smallest, and the maximum deviation was 4.25 MW. Figure A4b shows the results of the total thermal power deviation in each time period. The overall deviation of the scheduling was relatively large, the maximum deviation was 14.58 MW, the minimum deviation was at 6 o'clock, and the deviation was 0.56 WM at that moment. The smallest deviation was the real-time scheduling scheme, the maximum deviation was 1.89 WM, and the minimum deviation was 0 WM. It can be seen that the use of multi-time scale scheduling had an excellent performance regardless of the system power consumption or stability, which meets the requirements of wind-hydrogen integrated energy-saving development.

5. Conclusions

In the context of carbon trading, the impact of integrated energy-system scheduling on the ecological environment and on energy conservation was analyzed. The traditional wind-hydrogen integrated energy system has randomness and uncertainty in its operation which cannot meet the requirements of energy consumption and the economy. Therefore, the wind-hydrogen integrated system was analyzed and a multi-time scale optimal scheduling model of the system was established. Considering that the scheduling model is a multiobjective and nonlinear problem, the AFS-SFLA algorithm was combined with the frog leap algorithm to solve the scheduling model. The performance simulation test shows that in the multialgorithm test of the Rosenbrock function, the AFS-SFLA algorithm was better than the SFLA algorithm in the early iteration effect and tended to converge after 120 iterations. At that moment, the best solution was -0.436 . In the output power results of the integrated energy system in different periods, the daily scheduling, rolling scheduling, and real-time scheduling were basically consistent among the output power of the cogeneration. However, in the output power of the fan, the daily scheduling fluctuated greatly between the time period 0–3 and the time period 20–22, and the total output of power consumption of the daily scheduling scheme was relatively high. At 12:00, the output power of day ahead dispatching, rolling dispatching, and real-time dispatching was 14.6 MW, 2.3 MW, and 2.2 MW, respectively. In the multiperiod total thermal power deviation test, the overall deviation of the day ahead dispatching was large, with a maximum deviation of 14.58 MW. The real-time dispatching scheme had the smallest deviation, with a maximum deviation of 1.89 WM. It can be seen that the time-scale scheduling scheme had lower power consumption and stronger system stability than the traditional scheduling scheme. In the context of carbon trading, improving the comprehensive energy scheduling performance is of great significance for improving the stability of the energy system and reducing the energy consumption of the energy system. Therefore, this research established

a scheduling model with multiple time scales by analyzing the existing integrated energy system, and innovatively used the fish school algorithm and leapfrog algorithm to solve the problem. Finally, the stable operation of the integrated energy system was realized. However, considering the economic principle, the equipment used was mainly from the perspective of environmental protection and low carbon, without considering the impact of more comprehensive scheduling factors. Further improvement and optimization are required in the future to meet the needs of power grid development.

Author Contributions: Conceptualization, X.W.; methodology, X.W.; software, X.W. and B.S.; validation, X.W., B.S. and B.G.; formal analysis, X.W. and B.S.; investigation, X.W. and B.G.; resources, X.W.; data curation, X.W. and Y.L.; writing—original draft preparation, X.W.; writing—review and editing, X.W. and Y.L.; visualization, X.W.; supervision, B.G.; funding acquisition, X.W. All authors have read and agreed to the published version of the manuscript.

Funding: The work was financially supported by the 2022 Open Fund Project of the State Key Laboratory of Power Grid Safety and Energy Conservation (research on the low carbon economy operation model of integrated wind and hydrogen energy systems considering carbon trading, DZB51202201565).

Data Availability Statement: The data used to support the findings of this study are available from the corresponding author upon request.

Conflicts of Interest: The authors declare no conflict of interest.

Appendix A

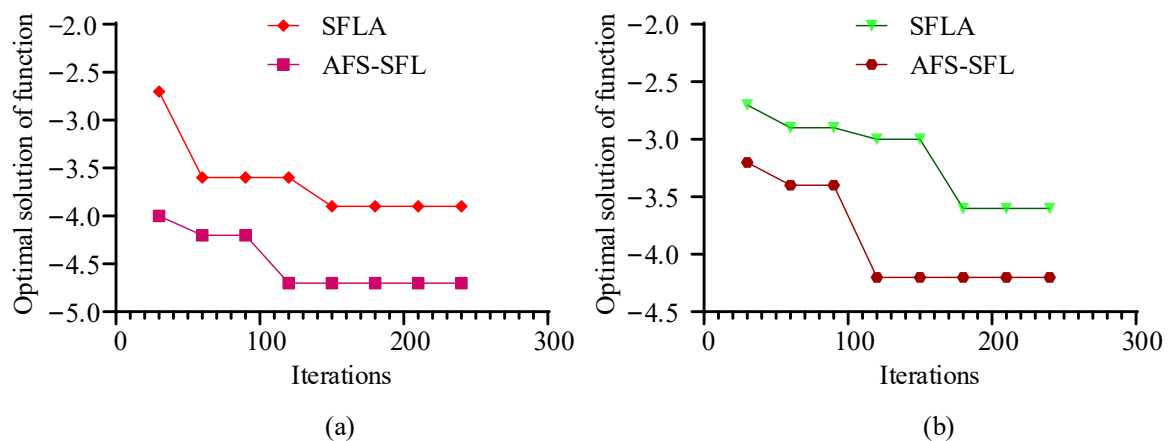


Figure A1. Test results under two benchmark functions (a). Optimal solution of Griewank function, (b). Optimal solution of Rosenbrock function.

Table A1. Testing the algorithm performance in dimension d .

Function Type	Result	AFS ($d = 20$)	AFS ($d = 50$)	AFS-SFLA ($d = 20$)	AFS-SFLA ($d = 50$)
Griewank	Optimal value	0.0015	0.0082	0.0010	0.0008
	Average value	0.0041	0.0112	0.0014	0.0004
Rosenbrock	Optimal value	0.0017	12.115	0.0013	0
	Average value	0.0265	18.735	0.0016	0

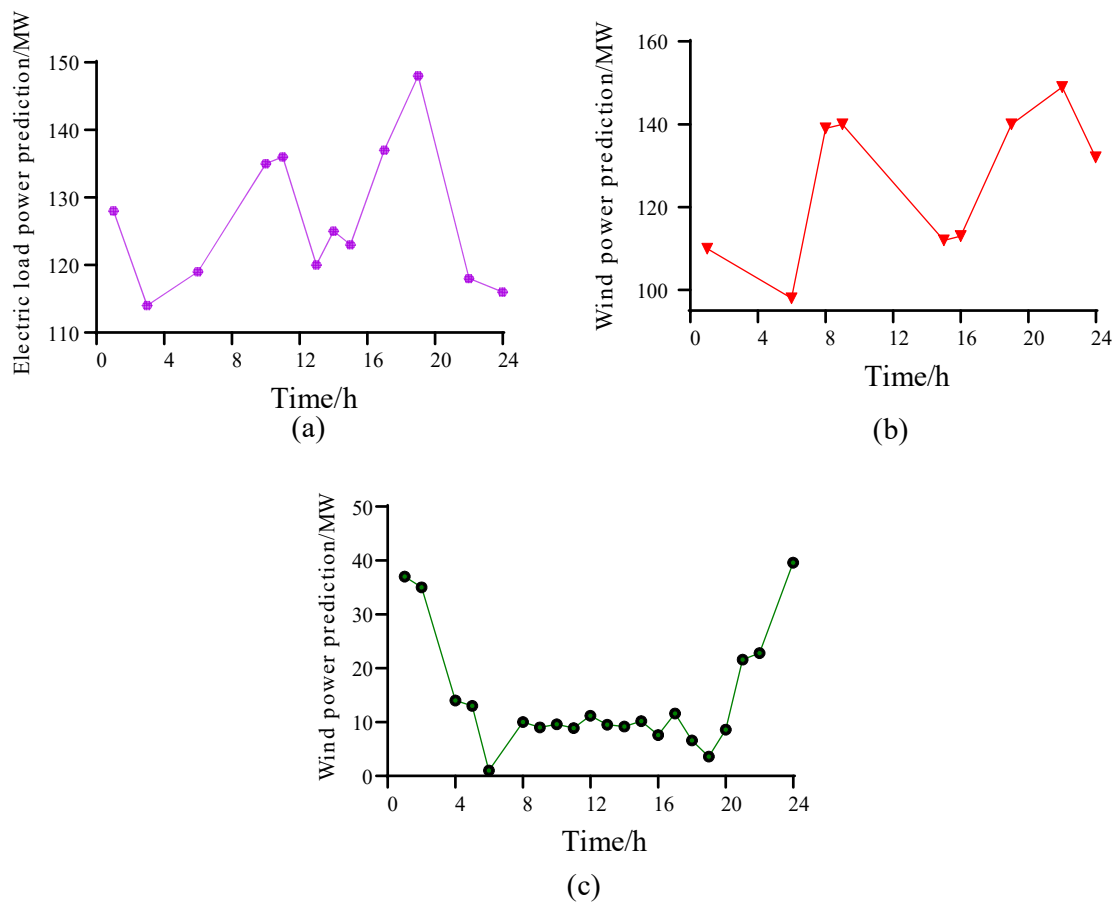


Figure A2. Typical daily load power forecast results (a). Electric load power prediction, (b). Thermal load power prediction, (c). Wind power prediction.

Table A2. Forecast error in different periods.

Test Category	Short-Term Forecast Error/%	Forecast Error in Expansion Period/%	Ultra-Short-Term Prediction Error/%
Thermal load	5	1	0.4
Electrical load	4	2	0.3
Wind power output	19	8	2.1

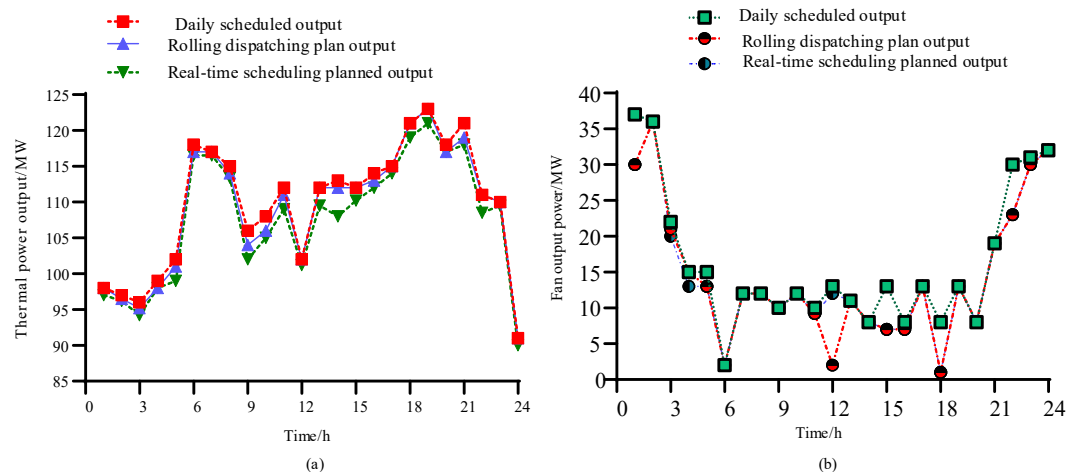
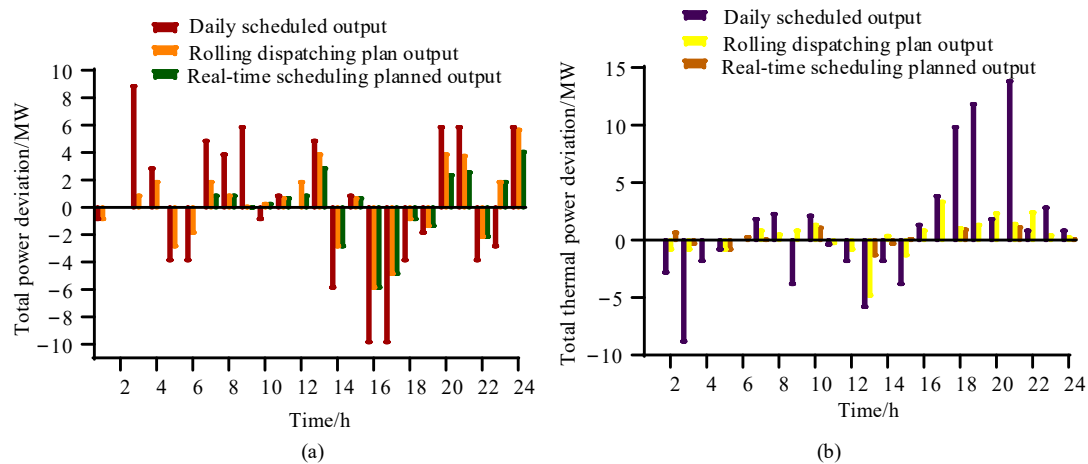


Figure A3. The results of the power data of the comprehensive energy system in different periods (a). Thermal power output, (b). Fan output power.

Table A3. The results of the electricity consumption test of the multiperiod integrated energy system.

Time Scale	Wind Power Consumption (/MW·h)	Consumption Rate of Wind Power/%
Day-ahead scheduling	341.45	93.54%
Rolling scheduling	342.54	94.65%
Real-time scheduling	350.64	97.45%

**Figure A4.** The deviation results of total electric power and longitudinal thermal power of the system at different time scales (a). Total electric power deviation results in each period, (b). Total thermal power deviation results in each period.

References

1. Rezaei, M.; Khalilpour, K.R.; Mohamed, M.A. Co-production of electricity and hydrogen from wind: A comprehensive scenario-based techno-economic analysis. *Int. J. Hydrog. Energy* **2021**, *46*, 18242–18256. [[CrossRef](#)]
2. Solomin, E.; Kirpichnikova, I.; Amerkhanov, R.; Korobov, D.; Lutovats, M.; Martyanov, A. Wind-hydrogen standalone uninterrupted power supply plant for all-climate application. *Int. J. Hydrog. Energy* **2019**, *44*, 3433–3449. [[CrossRef](#)]
3. Akhavan Shams, S.; Ahmadi, R. Dynamic optimization of solar-wind hybrid system connected to electrical battery or hydrogen as an energy storage system. *Int. J. Energy Res.* **2021**, *45*, 10630–10654. [[CrossRef](#)]
4. Ozturk, M.; Dincer, I. A comprehensive review on power-to-gas with hydrogen options for cleaner applications. *Int. J. Hydrog. Energy* **2021**, *46*, 31511–31522. [[CrossRef](#)]
5. Ishaq, H.; Dincer, I.; Crawford, C. A review on hydrogen production and utilization: Challenges and opportunities. *Int. J. Hydrog. Energy* **2022**, *47*, 26238–26264. [[CrossRef](#)]
6. Ishaq, H.; Dincer, I. Dynamic analysis of a new solar-wind energy-based cascaded system for hydrogen to ammonia. *Int. J. Hydrog. Energy* **2020**, *45*, 18895–18911. [[CrossRef](#)]
7. Yi, Z.; Xu, Y.; Zhou, J.; Wu, W.; Sun, H. Bi-level programming for optimal operation of an active distribution network with multiple virtual power plants. *IEEE Trans. Sustain. Energy* **2020**, *11*, 2855–2869. [[CrossRef](#)]
8. Xu, D.; Wu, Q.; Zhou, B.; Li, C.; Bai, L. Distributed multi-energy operation of coupled electricity, heating, and natural gas networks. *IEEE Trans. Sustain. Energy* **2019**, *11*, 2457–2469. [[CrossRef](#)]
9. Pan, G.; Gu, W.; Lu, Y.; Qiu, H.; Lu, S.; Yao, S. Optimal planning for electricity-hydrogen integrated energy system considering power to hydrogen and heat and seasonal storage. *IEEE Trans. Sustain. Energy* **2020**, *11*, 2662–2676. [[CrossRef](#)]
10. Dou, X.; Wang, J.; Wang, Z.L.; Bai, L.; Ren, S.; Gao, M. A dispatching method for integrated energy system based on dynamic time-interval of model predictive control. *J. Mod. Power Syst. Clean Energy* **2020**, *8*, 841–852. [[CrossRef](#)]
11. Lu, S.; Gu, W.; Zhang, C.; Meng, K.; Dong, Z. Hydraulic-thermal cooperative optimization of integrated energy systems: A convex optimization approach. *IEEE Trans. Smart Grid* **2020**, *11*, 4818–4832. [[CrossRef](#)]
12. Yang, W.; Liu, W.; Chung, C.Y.; Wen, F. Coordinated planning strategy for integrated energy systems in a district energy sector. *IEEE Trans. Sustain. Energy* **2019**, *11*, 1807–1819. [[CrossRef](#)]
13. Ospina, J.; Gupta, N.; Newaz, A.; Harper, M.; Faruque, M.O.; Collins, E.G.; Meeker, R.; Lofman, G. Sampling-based model predictive control of PV-integrated energy storage system considering power generation forecast and real-time price. *IEEE Power Energy Technol. Syst. J.* **2019**, *6*, 195–207. [[CrossRef](#)]

14. Gholamian, E.; Hanafizadeh, P.; Habibollahzade, A.; Ahmadi, P. Evolutionary based multi-criteria optimization of an integrated energy system with SOFC, gas turbine, and hydrogen production via electrolysis. *Int. J. Hydrog. Energy* **2018**, *43*, 16201–16214. [[CrossRef](#)]
15. Li, Y.; Han, M.; Yang, Z.; Li, G. Coordinating flexible demand response and renewable uncertainties for scheduling of community integrated energy systems with an electric vehicle charging station: A bi-level approach. *IEEE Trans. Sustain. Energy* **2021**, *12*, 2321–2331. [[CrossRef](#)]
16. Bhattacharjee, S.; Sioshansi, R.; Zareipour, H. Benefits of strategically sizing wind-integrated energy storage and transmission. *IEEE Trans. Power Syst.* **2020**, *36*, 1141–1151. [[CrossRef](#)]
17. Ruiming, F. Multi-objective optimized operation of integrated energy system with hydrogen storage. *Int. J. Hydrog. Energy* **2019**, *44*, 29409–29417. [[CrossRef](#)]
18. Shen, F.; Ju, P.; Shahidehpour, M.; Li, Z.; Wang, C.; Shi, X. Singular perturbation for the dynamic modeling of integrated energy systems. *IEEE Trans. Power Syst.* **2019**, *35*, 1718–1728. [[CrossRef](#)]
19. Mao, S.; Tang, Y.; Dong, Z.; Tang, Y.; Dong, Z.; Meng, K. A privacy preserving distributed optimization algorithm for economic dispatch over time-varying directed networks. *IEEE Trans. Ind. Inform.* **2020**, *17*, 1689–1701. [[CrossRef](#)]
20. Hosseini-Hemati, S.; Sheisi, G.H.; Karimi, S. Allocation-based optimal reactive power dispatch considering polynomial load model using improved grey wolf optimizer. *Iranian J. Sci. Technol. Trans. Electr. Eng.* **2021**, *45*, 921–944. [[CrossRef](#)]
21. Li, C.; Li, P.; Yu, H.; Li, H.; Zhao, J.; Li, S.; Wang, C. Optimal planning of community integrated energy station considering frequency regulation service. *J. Mod. Power Syst. Clean Energy* **2021**, *9*, 264–273. [[CrossRef](#)]
22. Chen, C.; Deng, X.; Zhang, Z.; Liu, S.; Waseem, M.; Dan, Y.; Lan, Z.; Lin, Z.; Yang, L.; Ding, Y. Optimal day-ahead scheduling of multiple integrated energy systems considering integrated demand response, cooperative game and virtual energy storage. *IET Gener. Transm. Distrib.* **2021**, *15*, 1657–1673. [[CrossRef](#)]
23. Gu, N.; Wang, H.; Zhang, J.; Wu, C. Bridging chance-constrained and robust optimization in an emission-aware economic dispatch with energy storage. *IEEE Trans. Power Syst.* **2021**, *37*, 1078–1090. [[CrossRef](#)]
24. Younes, Z.; Alhamrouni, I.; Mekhilef, S.; Rezasudin, M. A memory-based gravitational search algorithm for solving economic dispatch problem in micro-grid. *Ain Shams Eng. J.* **2021**, *12*, 1985–1994. [[CrossRef](#)]
25. Xi, L.; Zhou, L.; Liu, L.; Duan, D.; Xu, Y.; Yang, L.; Wang, S. A deep reinforcement learning algorithm for the power order optimization allocation of AGC in interconnected power grids. *CSEE J. Power Energy Syst.* **2020**, *6*, 712–723.
26. Vahedipour-Dahraie, M.; Rashidizadeh-Kermani, H.; Shafie-Khah, M.; João, P.S. Catalão. Risk-averse optimal energy and reserve scheduling for virtual power plants incorporating demand response programs. *IEEE Trans. Smart Grid* **2020**, *12*, 1405–1415. [[CrossRef](#)]
27. Lin, L.; Guan, X.; Peng, Y.; Wang, N.; Maharjan, S.; Ohtsuki, T. Deep reinforcement learning for economic dispatch of virtual power plant in internet of energy. *IEEE Internet Things J.* **2020**, *7*, 6288–6301. [[CrossRef](#)]
28. Li, Q.; Zhang, X.; Guo, J.; Shan, X.; Wang, Z.; Li, Z.; Tse, C.K. Integrating reinforcement learning and optimal power dispatch to enhance power grid resilience. *IEEE Trans. Circuits Syst. II: Express Briefs* **2021**, *69*, 1402–1406. [[CrossRef](#)]

Disclaimer/Publisher’s Note: The statements, opinions and data contained in all publications are solely those of the individual author(s) and contributor(s) and not of MDPI and/or the editor(s). MDPI and/or the editor(s) disclaim responsibility for any injury to people or property resulting from any ideas, methods, instructions or products referred to in the content.